PCCP

PAPER

View Article Online
View Journal | View Issue

Cite this: *Phys. Chem. Chem. Phys.*, 2019, **21**, 26637

Ab initio insights into the structural, energetic, electronic, and stability properties of mixed $Ce_nZr_{15-n}O_{30}$ nanoclusters†

Priscilla Felício-Sousa, [a] Johnatan Mucelini, [a] Larissa Zibordi-Besse, [a] Karla F. Andriani, [a] Yohanna Seminovski, [b] Ronaldo C. Prati [c] and Juarez L. F. Da Silva *[a]

Mixed CeO_2–ZrO_2 nanoclusters have the potential to play a crucial role in nanocatalysis, however, the atomistic understanding of those nanoclusters is far from satisfactory. In this work, we report a density functional theory investigation combined with Spearman rank correlation analysis of the energetic, structural and electronic properties of mixed $Ce_nZr_{15-n}O_{30}$ nanoclusters as a function of the composition (n = 0, 1,. . .,14, 15). For instance, we found a negative excess energy for all putative global minimum $Ce_nZr_{15-n}O_{30}$ configurations with a minimum at about n = 6 (*i.e.*, nearly 40% Ce), in which both the oxygen anion surroundings and cation radii play a crucial role in the stability and distribution of the chemical species. We found a strong energetic preference of Zr^{4+} cations to occupy larger coordination number sites, *i.e.*, the nanocluster core region, while the Ce^{4+} cations are located near vacuum exposed O-rich regions. As expected, we obtained an almost linear decrease of the average bond lengths by replacing Ce^{4+} by Zr^{4+} cations in the $(ZrO_2)_{15}$ nanoclusters towards the formation of mixed $Ce_nZr_{15-n}O_{30}$ nanoclusters, which resulted in a shift towards higher vibrational frequencies. Besides, we also observed that the relative stability of the mixed oxides is directly correlated with the increase (decrease) of the Zr d-state (Ce f-state) contribution to the highest occupied molecular orbital with the increase of the Zr content, hence driving the gap energy towards higher values.

Received 27th August 2019,
Accepted 15th November 2019

DOI: 10.1039/c9cp04762j

rsc.li/pccp

Introduction

Cerium oxides (CeO_x, $1.5 < x < 2.0$) play a crucial role as promoters in three-way catalytic converters due to the efficient oxidation–reduction cycle between Ce^{4+} and Ce^{3+}.[1–3] Related to that, they have an outstanding ability to store excess oxygen under fuel-lean conditions and to release oxygen through vacancy formation under fuel-rich conditions, which implies an excellent oxygen storage capacity (OSC).[4,5] The thermal deactivation of those materials has been shown to be a critical and limiting problem related to the loss of the OSC at high-temperature levels, nevertheless a solution has been proposed since the 1980s by doping CeO_2 with smaller ionic radii cations such as Y^{3+}, Zr^{4+}, Si^{4+}, *etc.*[6]

The formation of CeO_2 mixed oxide solid solutions with different dopants can modulate not only the thermal stability but also both the redox and catalytic properties. For instance, the decrease of the sintering rate in those materials is often associated with the assistance of the reduction of Ce^{4+} to Ce^{3+}, generating so-called associated defects.[7] Thus, Cho[8] attributed two origins to those defects, which creates as well two distinct types of oxygen vacancies, intrinsic and extrinsic effects. In the former one, the neighboring oxygen anions in CeO_2 act as reducing agents, while in the last one the dopant cation promotes the change from Ce^{4+} to Ce^{3+}.[6] However, both defects can be enhanced with the use of different undersized and non-reducible cations.

Among all possible cations, a mixture of CeO_2 with zirconium oxide, ZrO_2, which has higher thermal stability, smaller cations, and exceptional mechanical strength, appears to be a natural choice.[5,7] Furthermore, as expected, the formation of mixed

[a] *São Carlos Institute of Chemistry, University of São Paulo, PO Box 780, 13560-970, São Carlos, São Paulo, Brazil. E-mail: juarez_dasilva@iqsc.usp.br*
[b] *Instituto de Tecnología Química, Universitat Politècnica de València, Avda. de los Naranjos s/n, 46022 Valencia, Spain*
[c] *Center of Mathematics, Computer Science and Cognition, Federal University of ABC, Av. dos Estados, 5001, 09210-580, Santo André, SP, Brazil*

† Electronic supplementary information (ESI) available: Definitions of the structural properties employed to characterize the nanoclusters, comparison of the PBE and HSE06 functionals for selected structures, additional Spearman's correlation analysis, and the (x,y,z) coordinates of the nanoclusters with the lowest excess energy for all compositions. See DOI: 10.1039/c9cp04762j

CeO_2–ZrO_2 solid solutions can not only enhance the thermal stability but also tailor the system redox properties, once the inter-conversion of Ce^{4+} and Ce^{3+} is promoted, which is associated with the creation of oxygen vacancies in reactive environments.[4,5,7,9]

Most of the studies on ceria–zirconia solid solutions have focused on particular compositions of the bulk and surfaces,[10–12] but not of nanoclusters. For instance, the addition of zirconia in the CeO_2-bulk increases the channel diameter and hence favors oxygen migration in the lattice, raising progressive structural defects due to oxygen sub-lattice distortion and destabilization.[7,13] Along with those structural mismatches, a reduction of the coordination number from eight to sixfold for Zr^{4+} cations, as well as Zr–O bond distances increases, occurs due to the formation of oxygen anions neighboring the Zr^{4+} cations, and in conjunction those features promote more extensive oxygen mobility and improve the reducibility.

Furthermore, the aforementioned distortion and destabilization of the oxygen sub-lattice are minimized due to the formation of ZrO_2 and CeO_2-rich domains, creating meta-stable states, mainly at Zr-rich compositions.[13,14] For instance, Yang *et al.*[11] showed that the formation of oxygen vacancies at the $CeO_2(111)$ surface exactly occurs as observed for the ceria–zirconia bulk, in which the oxygen vacancies are formed close to Zr^{4+} cations, which led to the reduction of Ce^{4+} to Ce^{3+} as it also promotes larger structural defects. The most relevant result of this study showed that the oxygen vacancies have lower reduction energy and hence are more stable as compared with the CeO_2 surface. However, Zr-doped ceria surfaces are more stable in comparison with the CeO_2–ZrO_2 bulk.[15]

Ceria–zirconia nanoclusters should present some features of their precursors, although they are modulated in both composition and particle size. Zhang *et al.*[16] using high resolution transmission electron microscopy (TEM), X-ray diffraction (XRD) and Raman spectroscopy techniques at different temperature levels showed that the increase of zirconia content in $(1 - x)CeO_2$–$xZrO_2$ at the same temperature expands the particle size until reaching the amount of zirconia related to the phase transition between the cubic fluorite and tetragonal structures. For example, at 800 °C the particle size decreased from 15.7 nm to 5.4 nm, and from 50% of ZrO_2 an increase is observed due to the tetragonal phase formation. Conversely, an increase in the particle size from 16 nm to 81 nm is observed with an increment in the annealing temperature from 800 °C to 250 °C, forming compositions of the tetragonal phase, and hence those nanoclusters exhibit different phases from those expected from the bulk in CeO_2–ZrO_2.

Thus, there are several open questions regarding mixed ceria–zirconia nanoclusters, especially in the small nanoscale regime ($\leq$2 nm). Does zirconia play a crucial role in modulating the system properties? Is the most stable structure rich in zirconia or ceria? Are oxygen anions only plain spectators in the system stability? To address these and other questions, we aim in the present study to elucidate the structural, energetic and electronic properties of $Ce_nZr_{15-n}O_{30}$ for n = 0, 1,...,14, 15 mixed oxide clusters using *ab initio* density functional theory (DFT) calculations.

Theoretical approach and computational details

Total energy calculations

Our *ab initio* calculations were based on spin-polarized DFT within the exchange–correlation functional proposed by Perdew–Burke–Ernzenhof (PBE),[17] which is expected to provide a good description of Ce-based systems in which there are only Ce atoms in the +IV oxidation state, *i.e.*, the Ce 4f-states are delocalized.[18] Furthermore, as obtained by DFT+U calculations for $Zr_n/CeO_2(111)$, all Zr atoms are also in the +IV oxidation state,[12] and hence the Ce and Zr cations are both in the +IV oxidation state in the mixed CeO_2–ZrO_2 oxides. For the putative global minimum configurations (pGMCs) of the $Ce_nZr_{15-n}O_{30}$ nanoclusters, we employed also the hybrid functional proposed by Heyd–Scuseria–Ernzerhof (HSE06)[19,20] with the aim to obtain an improved description of the $Ce_nZr_{15-n}O_{30}$ properties, namely the excess energy, the energy separation between the highest occupied molecular orbital (HOMO) and lowest unoccupied molecular orbital (LUMO), E_{gap}, *etc.* (see the ESI†).

The Kohn–Sham molecular orbitals were expanded into numerical atom-centered orbitals (NAOs)[21,22] to solve the KS equations, as implemented in the all-electron full-potential Fritz-Haber Institute *ab initio* molecular simulations (FHI-aims) package.[21,23] For the NAOs, we employed the second improvement level basis set known as light-tier2 (adopting the FHI-aims terminology) for Ce, Zr and O species. The atomic zeroth-order relativistic approximation (atomic ZORA) was employed to take into account relativistic effects.[24]

For all calculations, electronic self-consistency was achieved once the total energy and forces were smaller than 1.0×10^{-6} eV and 2.5×10^{-3} eV Å^{-1}, respectively. A Gaussian broadening parameter of 0 meV was used to minimize fractional occupations of the HOMO and LUMO electronic states. The modified Broyden–Fletcher–Goldfarb–Shanno (BFGS) algorithm[23,25] was used to optimize the atomic forces on each atom, and the equilibrium geometry was obtained once the atomic forces on each atom were smaller than 2.5×10^{-2} eV Å^{-1}. Vibrational calculations were performed only for the pGMCs, which were verified as local minima by the absence of imaginary eigenvalues in the Hessian matrix.

Atomic structure configurations

For the designing of the trial configurations for the mixed CeO_2–ZrO_2 oxides, we selected four structures from our previous DFT-PBE study[26] for the $(CeO_2)_{15}$ and $(ZrO_2)_{15}$ systems, Fig. 1a, which include the pGMC and two high energy isomers (symmetric structures) derived from bulk fragments. The pGMCs were obtained using the tree-growth (TG) scheme combined with the Euclidean similarity distance (ESD) algorithm, and additional information about TG-ESD is discussed in the original reference.[26] For each selected composition, $Ce_nZr_{15-n}O_{30}$, n = 1,...,14, the trial configurations were designed using cation substitutions, as indicated in Fig. 1b. For example, several configurations were obtained for $Ce_1Zr_{14}O_{30}$ by the substitution of one of the Zr cations in the $(ZrO_2)_{15}$ structures in different

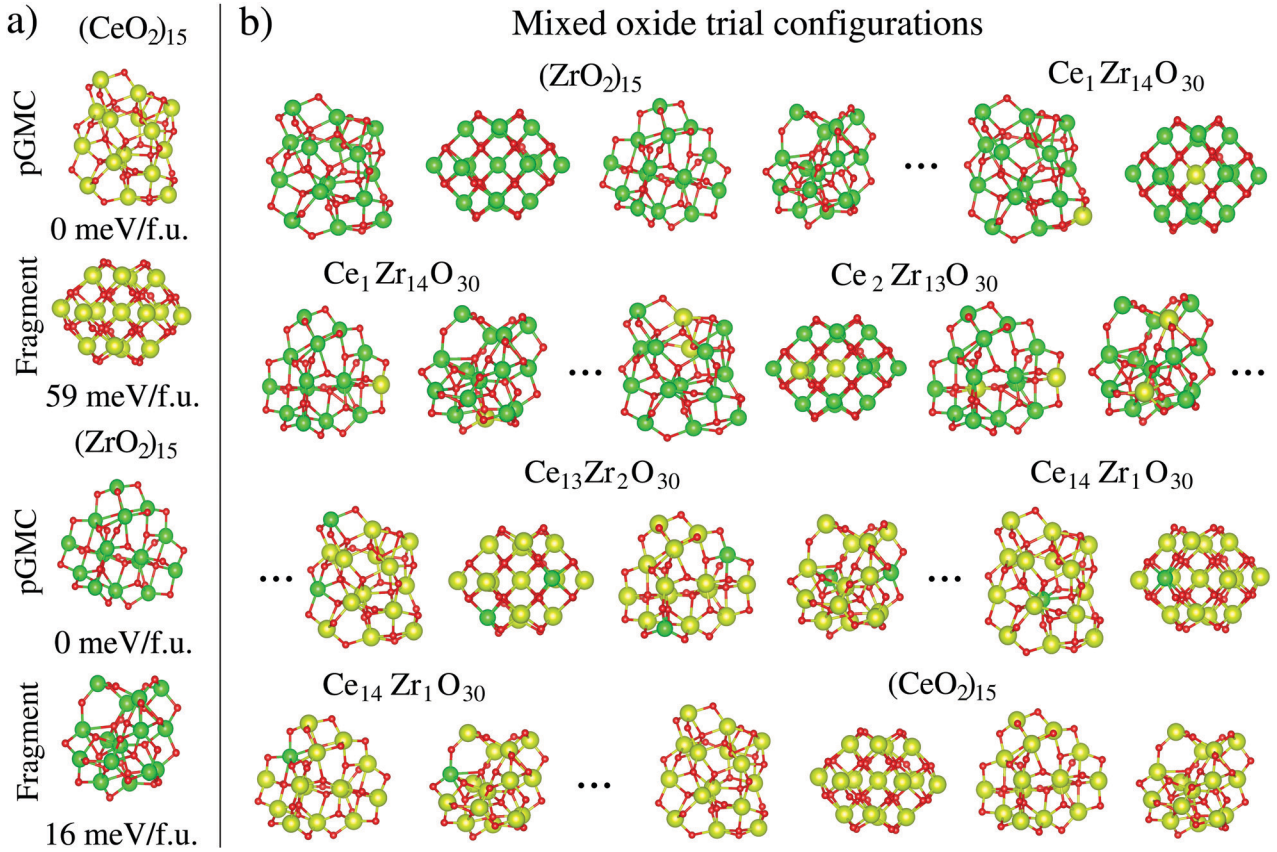

Fig. 1 (a) Selected structures for the $(CeO_2)_{15}$ and $(ZrO_2)_{15}$ nanoclusters obtained from our previous DFT-PBE study,[26] which includes the putative global minimum configurations (zero energy) and two high energy isomers derived from bulk fragments. (b) Mixed oxide trial configurations designed by cation substitutions in the four selected $(CeO_2)_{15}$ and $(ZrO_2)_{15}$ structures. Red, dark green, and light green spheres represent oxygen, zirconium, and cerium species, respectively.

locations within the nanocluster. The same procedure was repeated for all compositions and all selected structures, and in the end we obtained about 100 trial structures for each composition.

Spearman rank correlation

Along with this study, we calculated several physical and chemical properties to obtain atomistic insights into the mechanisms that drive the stability of mixed $Ce_nZr_{15-n}O_{30}$ nanoclusters, and hence a large amount of data was generated. With the aim to identify the most important trends among the structural, electronic, and energetic features for both pure and mixed oxides, we performed a statistical analysis based on the Spearman rank correlation coefficient,[27,28] which yields monotonic relationships among paired data. As a non-parametric technique for evaluating the degree of linear association or correlation within the data, r_s is not affected by the population distribution as it operates exclusively on the data ranks, which is suitable for our purpose.

The following formula was employed to calculate the Spearman rank correlation coefficient, r_s,

$$r_s = \frac{\mathrm{cov}(\mathrm{rg}_X, \mathrm{rg}_Y)}{\mathrm{sd}_{\mathrm{rg}_X}\mathrm{sd}_{\mathrm{rg}_Y}}, \quad (1)$$

where cov and sd are the covariance and the standard deviation function, while rg_X and rg_Y are rank values for the X and Y features' data. From its formulation, the r_s results are constrained within $-1 \leq r_s \leq +1$ values, where a positive (negative) value of r_s is obtained if y tends to increase (decrease) when x increases (increases). The monotonic correlation is stronger once the r_s values are closer to ± 1. Therefore, we investigated the correlations of several geometrical and electronic properties with the relative energy as features to indicate the stability of the mixed $Ce_nZr_{15-n}O_{30}$ oxides. Then, a positive/negative correlation may imply a preference of stable clusters to present a small/large property trend, whereas properties with small/significant correlation magnitude will affect marginally/mostly the mixed oxides' stability.

Results and discussion

Thus, following the procedures outlined above, we performed about 1651 geometric optimizations for the $Ce_nZr_{15-n}O_{30}$ (n = 0,...,15) oxides. The pGMCs obtained for each composition are shown in Fig. 2, while the atomic positions are reported within the ESI.† Below, we will discuss the energetics, structural, and

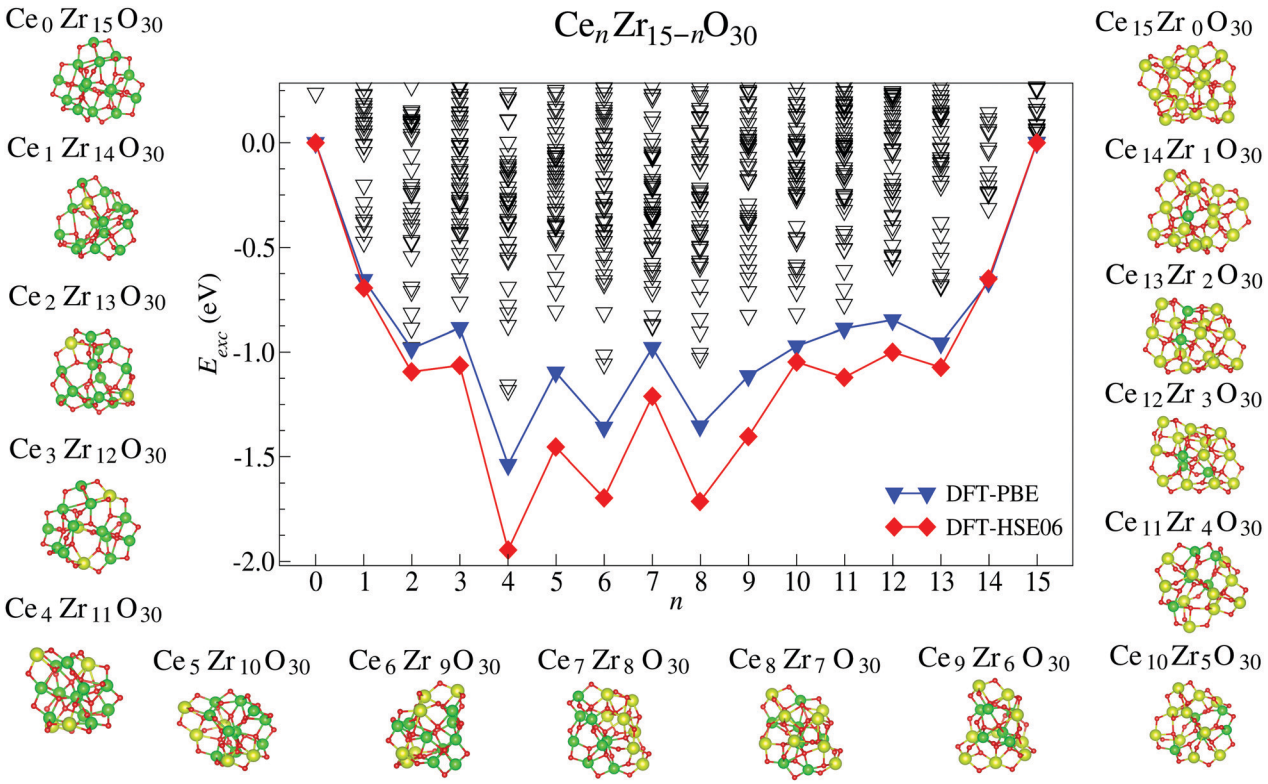

Fig. 2 Excess energy of mixed $Ce_nZr_{15-n}O_{30}$ nanoclusters, n = 0,...,15, with $Ce_{15}O_{30}$ and $Zr_{15}O_{30}$ as a reference (E_{exc} = 0 eV). Black triangles are the set of all PBE calculated structures, while blue triangles and red diamonds are the pGMCs obtained through PBE and HSE06, respectively. Blue and red solid lines are, respectively, the trends of E_{exc} for PBE and HSE06. The structures surrounding the graphic are the pGMCs for n = 0,...,15.

electronic properties as a function of the composition, as well as the Spearman rank correlation analysis.

Excess energy

The replacement of Zr cations within the $Zr_{15}O_{30}$ nanocluster by Ce can lower or increase the total energy, which plays a crucial role in the energetic stability of mixed nanoclusters. To address this question for all the studied compositions, we calculated the excess energy (mixing energy) at absolute zero, E_{exc}, which measures the relative energetic stability of a particular composition with respect to the parent nanoclusters (CeO_2, ZrO_2) in the respective pGMCs. Thus, E_{exc} was calculated using the following equation,

$$E_{exc} = E_{tot}^{Ce_nZr_{15-n}O_{30}} - (15-n)E_{tot}^{ZrO_2} - nE_{tot}^{CeO_2}, \qquad (2)$$

where $E_{tot}^{Ce_nZr_{15-n}O_{30}}$ indicates the total energy of the mixed oxide. $E_{tot}^{ZrO_2}$ and $E_{tot}^{CeO_2}$ are the total energies of zirconia and ceria pGMCs, respectively. By definition, E_{exc} = 0 for n = 0 and n = 15, while a negative (positive) value indicates an energetically favorable (unfavorable) composition. The results calculated for all configurations are shown in Fig. 2.

The excess energy is negative for all the pGMC mixed $Ce_nZr_{15-n}O_{30}$ nanoclusters, and hence their formation is energetically favorable compared with the separate systems, *i.e.*, CeO_2 and ZrO_2. However, since we set as a reference $(CeO_2)_{15}$ and $(ZrO_2)_{15}$ pGMCs (E_{exc} = 0 eV) in the excess energy formula, the configurations that were not derived from the pGMCs have high energies. For example, some of those configurations are derived from a fluorite bulk-like fragment which has higher energy than the pGMCs and for that reason originated high energy isomers with positive excess energy. Further details about the nature of the mixed oxide (pGMC) precursors are provided in Table S1 (ESI†). For instance, we found an increase in the stability (E_{exc} decreases) by successively replacing Zr within the selected $Zr_{15}O_{30}$ nanoclusters by Ce cations until the excess energy reaches a minimum at about n = 6 (*i.e.*, nearly 40% Ce) for both the PBE and HSE06 functionals, which is consistent with the experimental results.

For example, Lee *et al.*[13] suggested that the formation of $Ce_nZr_{15-n}O_{30}$ solid solutions is energetically favored due to the presence of CeO_2-rich and ZrO_2-rich domains. Thus ZrO_2-rich compositions are expected to be more stable as a result of the Zr cations' energetic preference to segregate or form a distinct Zr-rich phase as a stabilizing factor, especially at high-temperature.[2] There are differences in the magnitude of E_{exc} between the PBE and HSE06 results, *i.e.*, the HSE06 E_{exc} results are slightly lower in energy, but present the same trends. However, similar differences are expected as both functionals predict that all Ce atoms are in the oxidation state 4+. In this context, because the mixed $Ce_nZr_{15-n}O_{30}$ nanoclusters do not present any localized Ce 4f-states, we performed all posterior analyses with the PBE functional, which was shown to be suitable for the purpose of this present work.

Additional information about the performance between the PBE and HSE06 functionals for the investigated structural properties is provided in Fig. S2 (ESI†).

Insights into the relative energy stability from Spearman rank correlation

To obtain the stability–property relationship as a function of the $Ce_nZr_{15-n}O_{30}$ composition, we carried out the data treatment of all 1651 structures by using proper linear methods and the Spearman correlations for each data set. As show in Fig. 3, we represent the Spearman correlation analysis as a scatter plot matrix of the relative energy separated by chemical composition (columns) *versus* the most relevant structural and electronic features (rows), *i.e.*, the number of atoms (N), the average bond lengths (d_{av}), the energy gap (E_{gap}) and the absolute values of the HOMO and LUMO. To take into account the distinct atomic environments we separate the nanocluster regions into atoms located in the core (c) and vacuum exposed (v), which yielded new features, *e.g.*, $d_{av}^{O,v}$ indicates the average bond length of the oxygen atoms exposed to a vacuum. Thus, for all plots we considered only structures with relative energy smaller than 5 eV. However, analysis within smaller and larger relative energy windows drove us to the same conclusions as well as using Pearson and Kendall correlations as shown in Fig. S2 and S3 (ESI†), respectively.

We found that the formation of mixed $Ce_nZr_{15-n}O_{30}$ nanoclusters is favorable when a decrease of the number of Ce and Zr cations exposed to a vacuum is present, as show the positive correlation for $N^{Ce,v}$ and $N^{Zr,v}$. Thus, for the last one was found a higher angular coefficient as well as a better rank correlation, which indicates that Zr tends to be in the cluster core region rather than Ce cations. In addition, the opposite behaviour is observed for $N^{O,v}$; the negative correlation indicates the preference for the oxygen anions to be vacuum exposed, in particular with a small effective coordination number, ECN = 2 (see the ESI† for further details, *i.e.*, CN and ECN), as show the $N^{O,ECN2,v}$ plots. Conversely, the relative energy is minimized with a small number of oxygen atoms exposed to a vacuum with ECN = 3 as shows the negative correlation of $N^{O,ECN3,v}$.

Furthermore, our results indicate the preference of oxygen atoms with ECN = 2 to be vacuum exposed instead of oxygen atoms with ECN = 3 as observed in the stablest index surfaces of CeO_2 and ZrO_2[29,30] as well as on small nanoparticles of those

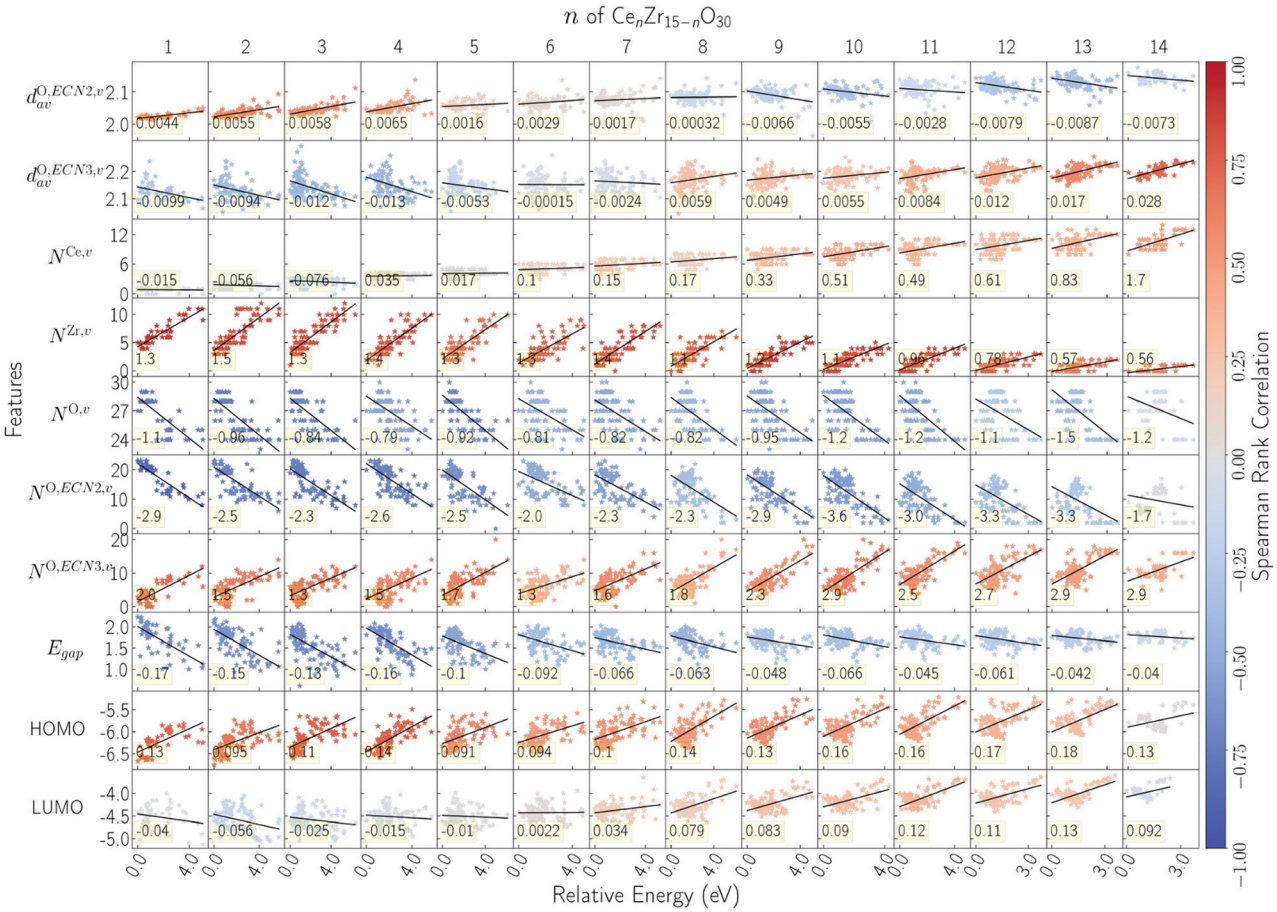

Fig. 3 A scatter plot matrix of the cluster relative energies (horizontal) against their electronic and structural features (vertical), where the different cluster properties and chemical compositions run over the rows and columns, respectively. Spearman's correlations are indicated in color and data linear fitting models with the respective angular coefficients are shown in the cells. We only considered structures with relative energy smaller than 5 eV.

materials.[31] An increment of $d_{av}^{O,ECN2,v}$ is observed for cerium-rich compositions, and hence an increase of $d_{av}^{O,ECN3,v}$ for zirconia-rich ones. As expected, the opposite behavior of $d_{av}^{O,ECN2,s}$ and $d_{av}^{O,ECN3,s}$ is observed for zirconia and cerium-rich compositions, respectively, which is in line with the number and coordination nature of the oxygen anions within the core and vacuum exposed. In addition, our results suggest that oxygen anions drive the increase of $N^{Ce,v}$ for cerium-rich compositions and the decrease of $N^{Zr,v}$ due to the preference for Zr–O interaction over Ce–O. Hence, Zr cations are prone to occupy specific larger CN sites, *i.e.*, the cluster core region, while Ce cations prefer small CN sites, *i.e.*, to be vacuum exposed.

Furthermore, we found that the electronic properties, namely the energy gap (E_{gap}) and the absolute value of the HOMO, are correlated with the relative stability of the mixed nanoclusters, while there is no significant correlation with the LUMO states, which is expected as they do not affect the nanoclusters' total energies, Fig. 3. The modulation of the relative energy by the HOMO states arises from the energetic contributions (kinetic and electrostatic) in the magnitude of the total energy, which explain the ascendant relation of those features. Conversely, the correlations between the band gap and relative energies are a direct result of the intrinsic correlation of the HOMO energies with E_{gap}, and hence the observed descendant relation is a consequence of the negative sign of the HOMO in the gap energy definition. Finally, our analysis showed that features that are driven by the cation radii and oxygen anions play a key role in modulating the mixed $Ce_nZr_{15-n}O_{30}$ oxide relative stability.

Structural properties

To improve our atomistic understanding of the formation of the mixed CeO_2 and ZrO_2 nanoclusters, we calculated the most important geometric parameters, namely the average bond lengths, d_{av}, coordination number, CN, chemical order parameter, σ, and average radius of the nanocluster. For d_{av} and CN, we also calculated the bonds lengths for each species, namely, d_{av}^{Ce}, d_{av}^{Zr}, d_{av}^{O}, *etc.* The results for $Ce_nZr_{15-n}O_{30}$ pGMCs are highlighted in Fig. 4, while all technical details are described within the ESI.† Furthermore, we calculated also the radial distribution function, RDF,

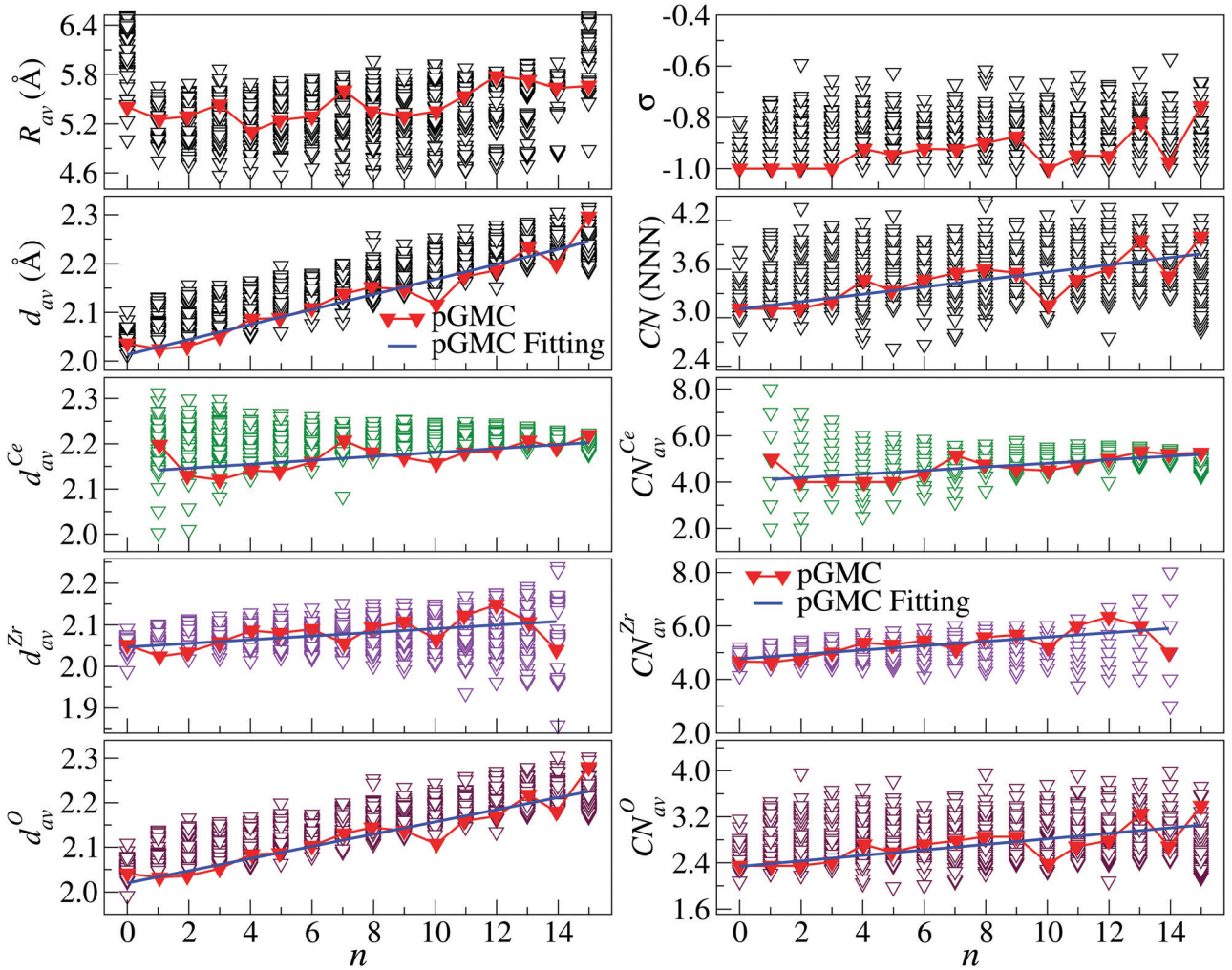

Fig. 4 Structural parameters for $Ce_nZr_{15-n}O_{30}$ clusters: average bond length, d_{av}, coordination number, CN (in next nearest neighbors – NNN), chemical order parameter, σ, and cluster radius R_{av}.

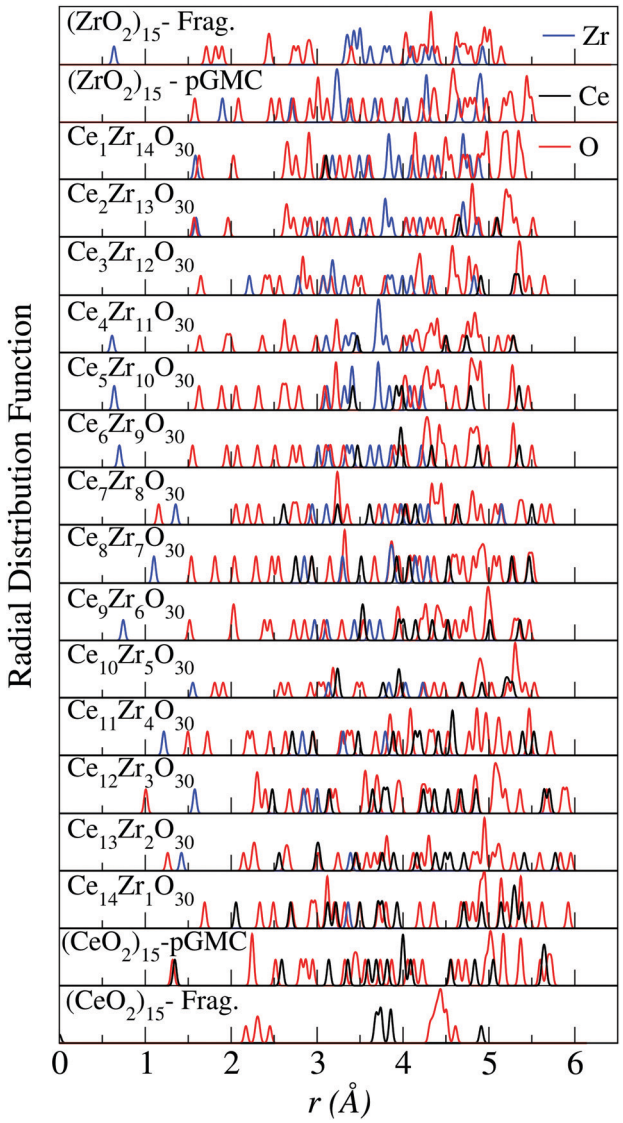

Fig. 5 Radial distribution function for $Ce_nZr_{15-n}O_{30}$ pGMCs, and $(CeO_2)_{15}$ and $(ZrO_2)_{15}$ bulk-like fragments in relation to the center of gravity. Black, blue and red solid lines are related to Ce, Zr and O atoms, respectively.

with respect to the geometric center for the mixed pGMCs, which is shown in Fig. 5.

We found an almost linear increase of the d_{av} values by replacing the Zr cations by Ce in the $(ZrO_2)_{15}$ nanocluster, which can be explained by the larger ionic radius of the Ce^{4+} cations (1.01 Å) compared with Zr^{4+} (0.86 Å).[32] In agreement with that, the average bond lengths of the O species to the cations, d_{av}^{O}, increases from 2.0 Å (pure ZrO_2) to 2.3 Å (pure CeO_2). Furthermore, from Fig. 4, we identified also small effects on the d_{av}^{Ce} and d_{av}^{Zr} results, while d_{av}^{O} captures the linear trends as the O bind to the Ce^{4+} and Zr^{4+} cations. The average coordination numbers, CN^{TM}, of both Ce and Zr species increase slightly by increasing the Ce composition, which can be clearly seen from the CN results. It can be explained by the higher coordination of the Ce^{4+} cations in ceria than for the Zr^{4+} cations in zirconia, *e.g.*, CN^{Ce} = 4.00 for $(CeO_2)_{15}$ and CN^{Zr} = 3.11 for $(ZrO_2)_{15}$.

The chemical order parameter, σ, was calculated for all optimized structures, and hence we found for all configurations σ values that spread from −1 (homogeneous distribution of the cations and anions) up to −0.6, *i.e.*, the number of hetero-atomic bonds is dominant, and hence there are no positive values for σ, which would indicate a tendency of phase separation between the anions and cations. For the particular case of the pGMCs, the composition affects slightly the σ results. For lower Ce composition (rich Zr, smaller x values), we found $\sigma = -1$, which is expected as we obtained the same values for bulk ZrO_2, however, there are small differences as the Ce composition increases, *i.e.*, changes from −1 to about −0.9, which can be explained by the reduction of the distance between the O–O anions within mixed nanoclusters for large Ce compositions, *i.e.*, similar to the results obtained for bulk CeO_2.

From the RDF results for the pGMCs, Fig. 5, we identified the following trends: (i) CeO_2 and ZrO_2 show clear differences, namely for CeO_2 there are well defined peaks, which indicate a more symmetric structure, which is not the case of ZrO_2; (ii) for the mixed oxide, we found an almost homogeneous distribution for the O species, as expected since the Ce and Zr cations bind only with the O; (iii) there is a strong energetic preference of the Zr cations for the core region of the mixed nanocluster, which can be explained by the smaller atomic radius of the Zr compared with the Ce cations; and (iv) the surface is dominated by oxygen species and corroborates with the Spearman correlation analysis, as expected based on the lower energy surfaces of those oxides, *e.g.*, CeO_2(111).

In conjunction, those structural properties could play a key role in the OSC of those types of materials, since one of the majors features that promote the oxygen vacancy formation is the contraction of the particle due to the increase of the undersized Zr content, leading to structural defects and displacement of not only the oxygen vacancies but also Ce and Zr cations, which is driven in $Ce_nZr_{15-n}O_{30}$ nanoclusters by not only the cation radii but also the coordination nature and number of the oxygen anions, as discussed in the previous sections. However, based on our findings, there is no uniform distribution of the cation species within the nanoclusters, which have also been shown to be a key factor for enhancing the OSC of CeO_2–ZrO_2 materials as well as the structural stability.[33,34]

Electronic properties

The results of Hirshfeld charge analysis[35,36] for the $Ce_nZr_{15-n}O_{30}$ pGMCs are shown in Fig. 6, where the following trends are observed: the zirconia doping gradually increases the positive charge over the Zr^{4+} cation, in general with lower magnitude than observed for the pure ZrO_2 bulk (0.71 *e*), resulting in a contraction of Zr–O bond lengths. Furthermore, the same effect is observed for Ce^{4+} cations, where the increase of the zirconia content has a positive effect on the Ce charges, becoming more positive in comparison with the CeO_2 bulk (0.68 *e*); this tendency also leads to a decrease of the Ce–O bond lengths in relation to the CeO_2 bulk. For instance, we observed a strong correlation between the charge and the location of the

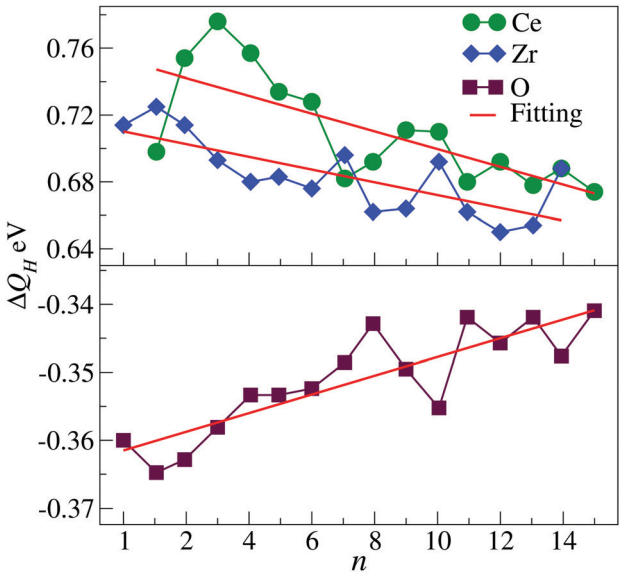

Fig. 6 Hirshfeld charges for $Ce_nZr_{15-n}O_{30}$ pGMCs, n = 0, 1,. . .,14, 15. The blue, green and brown lines are the charge per species for Zr, Ce and O, respectively, while the solid red line is the charge fitting.

O anions within the mixed oxide clusters as follows: the increase of the cation positive charge M = Ce or Zr decreases the M–O bond lengths with the increase of the cation content, which has a direct effect in modulating d_{av}^{O} and as a consequence the d_{av} trend.

The electronic properties of ceria and zirconia pGMCs including their composition derivatives were described through the projected density of states (pDOS), in which s-, p-, d- and f-states were plotted considering the dominant states for each atomic species as depicted in Fig. 7. The top panel displays the pDOS for the zirconia cluster, showing that the Zr d- and O p-states lie deeply in the valence band, in which the O p-states represented by the red lines are the dominant ones. On the contrary, the conduction band (unoccupied states) is mainly constituted by Zr d-states. We can observe that the gradual substitution of zirconium by cerium cations (middle panels) promotes changes in the valence states slightly until the $Ce_9Zr_6O_{30}$ composition, decreasing the contribution from the O 2p-states. However, from this composition the conduction states (unoccupied states) change significantly with the decrease of the Zr d-state contribution while the Ce d- and especially the Ce f-states have a more substantial contribution to the conduction band (right side). The gradual increase of Ce f-states with the n composition drives a gradual displacement of the HOMO–LUMO gap towards small HOMO–LUMO energy separations, E_{gap}, which forms more reactive species than the zirconia parent cluster (5.50 eV), as shown in the last panels. Conversely, the mixed nanoclusters' band gaps are always larger than the cerium parent cluster (3.74 eV), showing that an increase of the zirconium content stabilizes the mixed oxide structures.

Vibrational properties

The calculated vibrational infrared (IR) spectra for the $Ce_nZr_{15-n}O_{30}$ pGMCs, and $(CeO_2)_{15}$ and $(ZrO_2)_{15}$ bulk-like

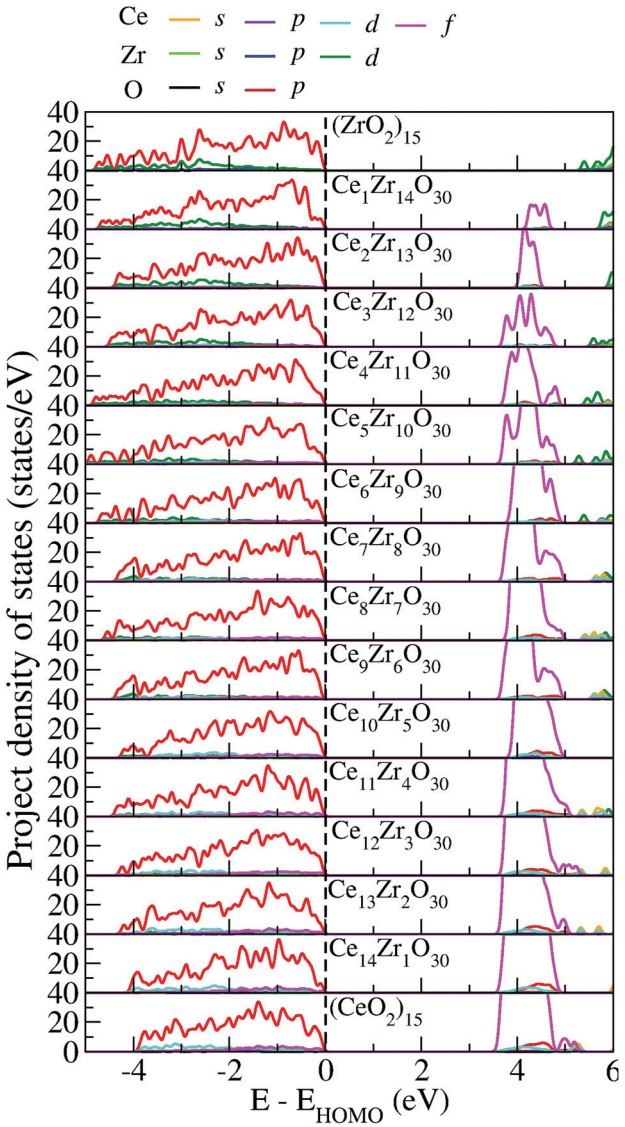

Fig. 7 Projected density of states as a function of composition for $Ce_nZr_{15-n}O_{30}$ pGMCs. The zero energy is located at the highest occupied molecular orbital.

fragments are shown in Fig. 8, and the following trends were identified: (i) compared with $Ce_{15}O_{30}$, the infrared spectra of $Zr_{15}O_{30}$ are displaced to higher frequencies. For example, the geometric center of the IR spectra is 625 cm^{-1} for $Zr_{15}O_{30}$, while it is 487 cm^{-1} for $Ce_{15}O_{30}$, *i.e.*, a shift of 138 cm^{-1}, which can be explained by the larger magnitude of the Zr–O binding compared with Ce–O.[26] Those results are consistent with the experimental observations, which found a band at 460 cm^{-1} with a shoulder around 430 cm^{-1} related to ceria nanoparticles similar to a fluorite structure.[37] (ii) Thus, as expected, the geometric center of the IR spectra shifts to lower energies by the replacement of Zr by Ce cations in the $(ZrO_2)_{15}$ structures, which is confirmed by our calculations. (iii) The differences in the vibrational infrared spectra using the pGMC and higher energy isomer structure derived from bulk fragments are small as most important structural features are present in both structures.

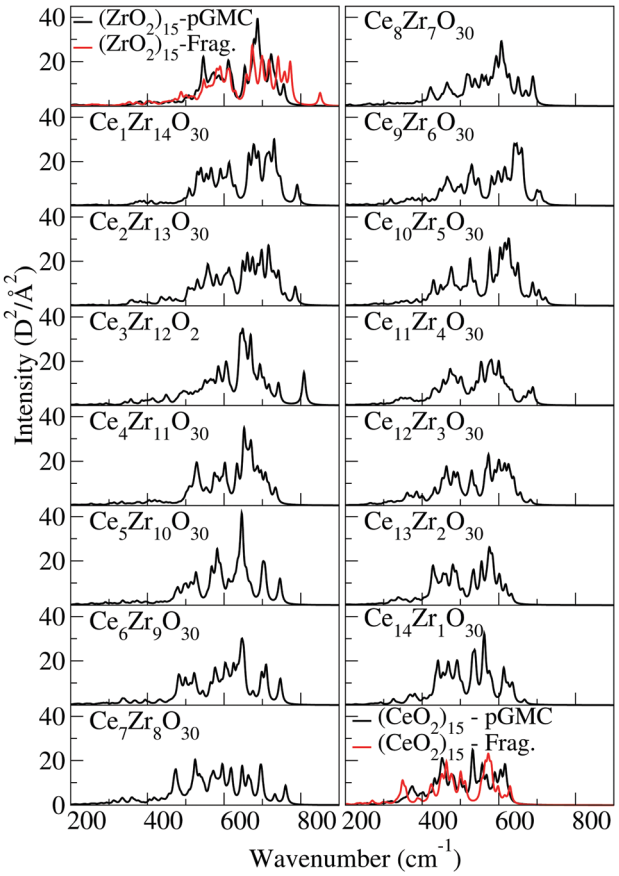

Fig. 8 Vibrational infrared spectra for the $Ce_nZr_{15-n}O_{30}$ pGMCs, and $(CeO_2)_{15}$ and $(ZrO_2)_{15}$ bulk-like fragments.

Conclusions

In this work, we reported a DFT-PBE/HSE06 investigation of the energetic, structural and electronic properties of mixed $Ce_nZr_{15-n}O_{30}$ nanoclusters as a function of composition, *e.g.*, n = 0, 1,...,14, 15, which can plays a crucial role in nanocatalysts. Beyond of the DFT calculations, we also explored the Spearman rank correlation analysis to obtain atomistic insights into the mechanisms that drive the relative stability of mixed $Ce_nZr_{15-n}O_{30}$ nanoclusters as a function of n = 0,...,15.

We found a negative excess energy for all putative global minimum $Ce_nZr_{15-n}O_{30}$ configurations with a minimum at about n = 6, which indicates an enhancement in the energetic stability due to the combination of CeO_2–ZrO_2 oxides, however, as expected, positive excess energy was also obtained for higher energy $Ce_nZr_{15-n}O_{30}$ isomers. Furthermore, the stabilization provided by enhancing the Zr content is due to the gradual displacement of the HOMO–LUMO gap towards larger energy separation as a direct result of the decrease of the Ce f-state and increase of the Zr d-state contribution, hence tuning the HOMO states to lower (negative) energies, in particular for Zr-rich compositions, *i.e.*, n = 1 to n = 6. In conjunction, our results showed that the cation radii and the oxygen environment play a crucial role in the energetic stability of the mixed nanoclusters.

For example, the Ce^{4+} cations have a larger atomic radius (1.01 Å) than the Zr^{4+} (0.86 Å) cations,[32] and hence there is a strong energetic preference of the Zr cations for the core region of the nanocluster, *i.e.*, they occupy specific larger CN sites, while the bigger Ce cations are located near O-rich regions and hence tend to be vacuum exposed, *i.e.*, occupy small CN sites. Moreover, following those findings, we obtained an almost linear decreasing of the bond lengths by replacing the Ce by Zr cations in the $(ZrO_2)_{15}$ nanoclusters due to the enhancement of the positive (negative) cation (anion) charges. In conjunction, those features resulted in a clear shift in the vibrational frequencies from lower to higher frequencies by the replacement of Ce by Zr cations, which can be explained by the stronger binding energy and the preference for Zr–O bonds, driven by the oxygen anions.

Conflicts of interest

There are no conflicts to declare.

Acknowledgements

The authors gratefully acknowledge support from FAPESP (São Paulo Research Foundation, Grant Number 2017/11631-2, 2018/11152-0), Shell and the strategic importance of the support given by ANP (Brazil's National Oil, Natural Gas and Biofuels Agency) through the R&D levy regulation. This study was financed in part by the Coordenacão de Aperfeiçoamento de Pessoal de Nível Superior – Brasil (CAPES) – Finance Code 001. The authors acknowledge also the National Laboratory for Scientific Computing (LNCC/MCTI, Brazil) for providing HPC resources of the SDumont supercomputer, which have contributed to the research results reported within this paper. URL: http://sdumont.lncc.br. JLFDS acknowledges the Advanced Scientific Computational Laboratory (University of São Paulo) and the infrastructure provided to our computer cluster by the São Carlos Center of Informatics, University of São Paulo.

Notes and references

1 A. Trovarelli, *Catalysis by Ceria and Related Materials*, World Scientific, London, 2002, vol. 2, p. 528.
2 R. Grau-Crespo, N. H. de Leeuw, S. Hamad and U. V. Waghmare, *Proc. R. Soc. London, Ser. A*, 2011, **467**, 1925–1938.
3 C. Sun, H. Li and L. Chen, *Energy Environ. Sci.*, 2012, **5**, 8475–8505.
4 T. Murota, T. Hasegawa and S. Aozasa, *J. Alloys Compd.*, 1993, **193**, 298–299.
5 R. D. Monte and J. Kašpar, *Catal. Today*, 2005, **100**, 27–35.
6 M. Pijolat, M. Prin, M. Soustelle, O. Touret and P. Nortier, *J. Chem. Soc., Faraday Trans.*, 1995, **91**, 3941–3948.
7 J. Kašpar, P. Fornasiero and M. Graziani, *Catal. Today*, 1999, **50**, 285–298.
8 B. Cho, *J. Catal.*, 1991, **131**, 74–87.

9 S. Hosokawa, S. Imamura, S. Iwamoto and M. Inoue, *J. Eur. Ceram. Soc.*, 2011, **31**, 2463–2470.
10 J. A. Rodriguez, J. C. Hanson, J.-Y. Kim, G. Liu, A. Iglesias-Juez and M. Fernández-García, *J. Phys. Chem. B*, 2003, **107**, 3535–3543.
11 Z. Yang, Y. Wei, Z. Fu, Z. Lu and K. Hermansson, *Surf. Sci.*, 2008, **602**, 1199–1206.
12 J. Mucelini, R. Costa-Amaral, Y. Seminovski and J. L. F. Da Silva, *J. Chem. Phys.*, 2018, **149**, 244702.
13 T. A. Lee, C. R. Stanek, K. J. McClellan, J. N. Mitchell and A. Navrotsky, *J. Mater. Res.*, 2008, **23**, 1105–1112.
14 G. Vlaic, P. Fornasiero, S. Geremia, J. Kašpar and M. Graziani, *J. Catal.*, 1997, **168**, 386–392.
15 Z. Yang, T. W. Woo, M. Baudin and K. Hermansson, *J. Chem. Phys.*, 2004, **120**, 7741–7749.
16 F. Zhang, C.-H. Chen, J. C. Hanson, R. D. Robinson, I. P. Herman and S.-W. Chan, *J. Am. Ceram. Soc.*, 2006, **89**, 1028–1036.
17 J. P. Perdew, K. Burke and M. Ernzerhof, *Phys. Rev. Lett.*, 1996, **77**, 3865–3868.
18 J. L. F. Da Silva, M. V. Ganduglia-Pirovano, J. Sauer, V. Bayer and G. Kresse, *Phys. Rev. B: Condens. Matter Mater. Phys.*, 2007, **75**, 045121.
19 J. Heyd, G. E. Scuseria and M. Ernzerhof, *J. Chem. Phys.*, 2003, **118**, 8207–8215.
20 J. Heyd, G. E. Scuseria and M. Ernzerhof, *J. Chem. Phys.*, 2006, **124**, 219906.
21 V. Blum, R. Gehrke, F. Hanke, P. Havu, V. Havu, X. Ren, K. Reuter and M. Scheffler, *Comput. Phys. Commun.*, 2009, **180**, 2175–2196.
22 V. Havu, V. Blum, P. Havu and M. Scheffler, *J. Comput. Phys.*, 2009, **228**, 8367–8379.
23 J. Nocedal and S. J. Wright, *Numerical Optimization*, Springer, New York, 2nd edn, 2006, p. 664.
24 E. van Lenthe, J. G. Snijders and E. J. Baerends, *J. Chem. Phys.*, 1996, **105**, 6505–6516.
25 W. H. Press, S. A. Teukolsky, W. T. Vetterling and B. P. Flannery, *Numerical Recipes: The Art of Scientific Computing*, Cambridge University Press, Cambridge, 3rd edn, 2007, p. 1256.
26 L. Zibordi-Besse, Y. Seminovski, I. Rosalino, D. Guedes-Sobrinho and J. L. F. Da Silva, *J. Phys. Chem. C*, 2018, **122**, 27702–27712.
27 C. Spearman, *Am. J. Psychol.*, 1904, **15**, 72–101.
28 T. Gauthier, *Environ. Forensics*, 2001, **2**, 359–362.
29 M. Nolan, S. C. Parker and G. W. Watson, *Surf. Sci.*, 2005, **595**, 223–232.
30 C. Ricca, A. Ringuedé, M. Cassir, C. Adamo and F. Labat, *J. Comput. Chem.*, 2014, **36**, 9–21.
31 Z. L. Wang and X. Feng, *J. Phys. Chem. B*, 2003, **107**, 13563–13566.
32 R. D. Shannon, *Acta Crystallogr., Sect. A: Cryst. Phys., Diffr., Theor. Gen. Crystallogr.*, 1976, **32**, 751–767.
33 Y. Nagai, T. Yamamoto, T. Tanaka, S. Yoshida, T. Nonaka, T. Okamoto, A. Suda and M. Sugiura, *Catal. Today*, 2002, **74**, 225–234.
34 T. Vinodkumar, D. Mukherjee, C. Subrahmanyam and B. M. Reddy, *New J. Chem.*, 2018, **42**, 5276–5283.
35 F. L. Hirshfeld, *Theor. Chim. Acta*, 1977, **44**, 129–138.
36 R. F. Nalewajski and R. G. Parr, *Proc. Natl. Acad. Sci. U. S. A.*, 2000, **97**, 8879–8882.
37 S. Damyanova, B. Pawelec, K. Arishtirova, M. M. Huerta and J. Fierro, *Appl. Catal., A*, 2008, **337**, 86–96.

